



Year: 2015

Measurement of the forward-backward asymmetry in $Z/\gamma^* \rightarrow \mu^+\mu^-$ decays and determination of the effective weak mixing angle

LHCb Collaboration ; Aaij, R ; Adeva, B ; Adinolfi, M ; Anderson, J ; Bernet, R ; Bowen, E ; Bursche, A ; Chiapolini, N ; Chrzaszcz, M ; Dey, B ; Elsasser, C ; Graverini, E ; Lionetto, F ; Lowdon, P ; Mauri, A ; Müller, K ; Serra, N ; Steinkamp, O ; Storaci, B ; Straumann, U ; Tresch, M ; Vollhardt, A ; Weiden, A ; et al

Abstract: The forward-backward charge asymmetry for the process $q\bar{q} \rightarrow Z/\gamma^* \rightarrow \mu^+\mu^-$ is measured as a function of the invariant mass of the dimuon system. Measurements are performed using proton proton collision data collected with the LHCb detector at $\sqrt{s} = 7$ and 8, corresponding to integrated luminosities of 1fb^{-1} and 2fb^{-1} respectively. Within the Standard Model the results constrain the effective electroweak mixing angle to be

$$\sin^2\theta_W^{eff} = 0.23142 \pm 0.00073 \pm 0.00052 \pm 0.00056$$

where the first uncertainty is statistical, the second systematic and the third theoretical. This result is in agreement with the current world average, and is one of the most precise determinations at hadron colliders to date.

DOI: [https://doi.org/10.1007/JHEP11\(2015\)190](https://doi.org/10.1007/JHEP11(2015)190)

Posted at the Zurich Open Repository and Archive, University of Zurich

ZORA URL: <https://doi.org/10.5167/uzh-122738>

Journal Article

Accepted Version

Originally published at:

LHCb Collaboration; Aaij, R; Adeva, B; Adinolfi, M; Anderson, J; Bernet, R; Bowen, E; Bursche, A; Chiapolini, N; Chrzaszcz, M; Dey, B; Elsasser, C; Graverini, E; Lionetto, F; Lowdon, P; Mauri, A; Müller, K; Serra, N; Steinkamp, O; Storaci, B; Straumann, U; Tresch, M; Vollhardt, A; Weiden, A; et al (2015). Measurement of the forward-backward asymmetry in $Z/\gamma^* \rightarrow \mu^+\mu^-$ decays and determination of the effective weak mixing angle. Journal of High Energy Physics, 2015(11):190.

DOI: [https://doi.org/10.1007/JHEP11\(2015\)190](https://doi.org/10.1007/JHEP11(2015)190)



CERN-PH-EP-2015-250

LHCb-PAPER-2015-039

24 September 2015

Measurement of the forward-backward asymmetry in $Z/\gamma^* \rightarrow \mu^+ \mu^-$ decays and determination of the effective weak mixing angle

The LHCb collaboration[†]

Abstract

The forward-backward charge asymmetry for the process $q\bar{q} \rightarrow Z/\gamma^* \rightarrow \mu^+ \mu^-$ is measured as a function of the invariant mass of the dimuon system. Measurements are performed using proton proton collision data collected with the LHCb detector at $\sqrt{s} = 7$ and 8 TeV, corresponding to integrated luminosities of 1 fb^{-1} and 2 fb^{-1} respectively. Within the Standard Model the results constrain the effective electroweak mixing angle to be

$$\sin^2 \theta_W^{\text{eff}} = 0.23142 \pm 0.00073 \pm 0.00052 \pm 0.00056,$$

where the first uncertainty is statistical, the second systematic and the third theoretical. This result is in agreement with the current world average, and is one of the most precise determinations at hadron colliders to date.

Published in JHEP 1511(2015) 190

© CERN on behalf of the LHCb collaboration, licence CC-BY-4.0.

[†]Authors are listed at the end of this paper.

1 Introduction

In the Standard Model (SM), the Z boson couplings differ for left- and right-handed fermions. The difference leads to an asymmetry in the angular distribution of positively and negatively charged leptons produced in Z boson decays. This asymmetry depends on the weak mixing angle (θ_W) between the neutral states associated to the U(1) and SU(2) gauge groups, i.e. the relative coupling strengths between the photon and the Z boson. In order to compare directly with previous experimental determinations, a scheme is adopted in which the higher order corrections to the Z boson couplings are absorbed in effective couplings. The resulting effective parameter $\sin^2\theta_W^{\text{eff}}$ is defined as a function of the ratio of the vector and the axial-vector effective couplings of the Z boson to the fermions involved [1], and is proportional to $\sin^2\theta_W$.

Defining θ^* as the polar angle of the negatively charged lepton in the Collins-Soper [2] frame, in which the direction of the z -axis is aligned with the difference of the incoming proton momentum vectors in the dimuon rest frame, the differential cross section in the SM at leading order is

$$\frac{d\sigma}{d\cos\theta^*} = A(1 + \cos^2\theta^*) + B\cos\theta^*.$$

Here A and B are coefficients that depend on the dimuon invariant mass, mainly because of interference between Z and γ^* contributions, the colour charge of the quarks and the vector and axial-vector couplings. The parameter B is a function of $\sin^2\theta_W$ and is proportional to the forward-backward asymmetry A_{FB} , which is given by

$$A_{\text{FB}} \equiv \frac{N_{\text{F}} - N_{\text{B}}}{N_{\text{F}} + N_{\text{B}}},$$

where N_{F} represents the number of forward decays ($\cos\theta^* > 0$) and N_{B} the number of backward decays ($\cos\theta^* < 0$). The Collins-Soper frame is used because it minimises the impact of the transverse momentum of the incoming quarks on the identification of forward and backward decays.

In this paper the asymmetry of the angular distribution of muons in $Z \rightarrow \mu^+\mu^-$ decays¹ is measured using proton proton collision data collected by the LHCb experiment at centre-of-mass energies of $\sqrt{s} = 7$ and 8 TeV, corresponding to an integrated luminosity of 1 fb^{-1} and 2 fb^{-1} respectively. The asymmetry as a function of the dimuon invariant mass is used to determine $\sin^2\theta_W^{\text{eff}}$.

Comparisons of the determinations of the weak mixing angle from processes with different initial and final state fermions provide a test of the universality of the fermion to Z couplings. The most accurate measurement of $\sin^2\theta_W^{\text{eff}}$ at the LEP experiments was obtained from the forward-backward asymmetry in b quark final states [1], and at the SLD experiment by measuring the left-right asymmetry with polarised electrons [3]. Determinations of $\sin^2\theta_W^{\text{eff}}$ have also been obtained in hadronic production processes with

¹In the following Z is used to denote the Z/γ^* contributions.

leptonic final states at the CDF and D0 experiments at the Tevatron [4, 5] and ATLAS and CMS experiments at the LHC [6, 7].

Measurements of A_{FB} can be related to $\sin^2\theta_{\text{W}}^{\text{eff}}$ when the momentum direction of the initial quark and antiquark are known. At the LHC the momentum direction of the initial-state quark is not known, diluting the ability to determine $\sin^2\theta_{\text{W}}^{\text{eff}}$ from A_{FB} . However, since at LHC the dominant production process is $u\bar{u}, d\bar{d} \rightarrow Z$, the main contribution originates from a collision of a valence quark with high momentum and a sea antiquark with lower momentum, and so the Z boson tends to be boosted along the direction of the quark. This is particularly true in the forward region where the Z boson has large longitudinal momentum. Consequently, the sensitivity of A_{FB} to $\sin^2\theta_{\text{W}}^{\text{eff}}$ is greater at large rapidities of the Z boson. Using simulated samples, it is found that in the LHCb acceptance the assignment of forward and backward decays is correct in 90% of the time.

The layout of this paper is as follows. Section 2 describes the LHCb detector and the data samples used in the analysis. The candidate selection and background determination are described in Sec. 3. In Sec. 4 the A_{FB} measurements are presented and in Sec. 5 the measurements are compared to next-to-leading order (NLO) theoretical predictions within the same kinematic region, and a value of $\sin^2\theta_{\text{W}}^{\text{eff}}$ is determined.

2 Detector and datasets

The LHCb detector [8, 9] is a single-arm forward spectrometer covering the pseudorapidity range $2 < \eta < 5$. The detector includes a high-precision tracking system consisting of a silicon-strip vertex detector surrounding the pp interaction region, a large-area silicon-strip detector located upstream of a dipole magnet with a bending power of about 4 Tm, and three stations of silicon-strip detectors and straw drift tubes placed downstream of the magnet. The magnet polarity can be reversed, so that detector-induced asymmetries can be studied and corrected for in the analyses. The tracking system provides a measurement of momentum, p , of charged particles with a relative uncertainty that varies from 0.5% at low momentum to 1.0% at 200 GeV.² The minimum distance of a track to a primary vertex, the impact parameter, is measured with a resolution of $(15 + 29/p_{\text{T}}) \mu\text{m}$, where p_{T} is the component of the momentum transverse to the beam, in GeV. Different types of charged hadrons are distinguished using information from two ring-imaging Cherenkov detectors. Photons, electrons and hadrons are identified by a calorimeter system consisting of scintillating-pad and preshower detectors, an electromagnetic calorimeter and a hadronic calorimeter. Muons are identified by a system composed of alternating layers of iron and multiwire proportional chambers. The online event selection is performed by a trigger, that consists of a hardware stage, based on information from the calorimeter and muon systems, followed by a software stage, which applies a full event reconstruction. For this analysis, candidates are triggered by at least one muon with momentum larger than 10 GeV.

Simulated samples are used to estimate the shapes of the invariant mass distributions for the simulated signal sample and some of the background sources. The signal sample is

²Units where the speed of light is set to unity are used throughout this paper.

also used to correct the data for reconstruction and detector effects. In the simulation, pp collisions are generated using PYTHIA 8 [10, 11] with a specific LHCb configuration [12]. Decays of hadronic particles are described by EVTGEN [13], in which final-state radiation (FSR) is generated using PHOTOS [14]. The interaction of the generated particles with the detector, and its response, are implemented using the GEANT4 toolkit [15], as described in Ref. [16].

To simulate $Z \rightarrow \mu^+ \mu^-$ decays with different values of $\sin^2 \theta_W^{\text{eff}}$, the next-to-leading order generator POWHEG-BOX [17], interfaced to PYTHIA for the parton showering, is used. Additional simulated samples are generated without parton showering using POWHEG-BOX, HERWIG [18] and FEWZ [19] and are used to evaluate theoretical uncertainties. Predictions are also obtained using FEWZ at NLO and are used to provide an alternative calculation of A_{FB} to compare to those computed by the POWHEG-BOX generator. The same parton density function (PDF) is used for both generators.

3 Event selection

Dimuon candidates, consisting of two oppositely charged muons, are selected using the same criteria as in Ref. [20], but with an extended mass range. The two muons must be within $2.0 < \eta < 4.5$, have good quality track fits, a transverse momentum greater than 20 GeV and must combine to an invariant mass within $60 < m_{\mu\mu} < 160$ GeV. These requirements define the kinematic region of this measurement.

The purity of the candidate sample is determined by estimating the contribution from background sources using a combination of simulation and data-driven techniques, and is found to be greater than 99%. The total yield, reconstructed dimuon invariant mass and A_{FB} are determined for each source of background.

The largest background contributions come from semileptonic heavy-flavour decays and events containing misidentified hadrons, where hadrons punching through the calorimeters to the muon stations are identified as muons, or hadrons have decayed in flight. Both contributions are estimated using data-driven techniques. Two heavy-flavour enriched samples are selected by widening the mass window and requiring evidence that (i) the muons are produced away from the primary vertex, or (ii) that the muons are surrounded by hadronic activity. These two samples are combined to estimate both the shape of the reconstructed $m_{\mu\mu}$ distribution and the total number of events for the heavy-flavour background source. The misidentified hadron contribution is estimated by using a sample of same-sign muon events. The $Z \rightarrow \tau^+ \tau^-$, $t\bar{t}$, single top and $W^+ W^- \rightarrow \mu^+ \nu_\mu \mu^- \bar{\nu}_\mu$ background sources are estimated using simulation. The total background contribution is largest at low invariant mass. The charge asymmetry of each background component is consistent with zero over the whole mass range. The distribution of the dimuon invariant mass is shown for data and all background sources in Fig. 1.

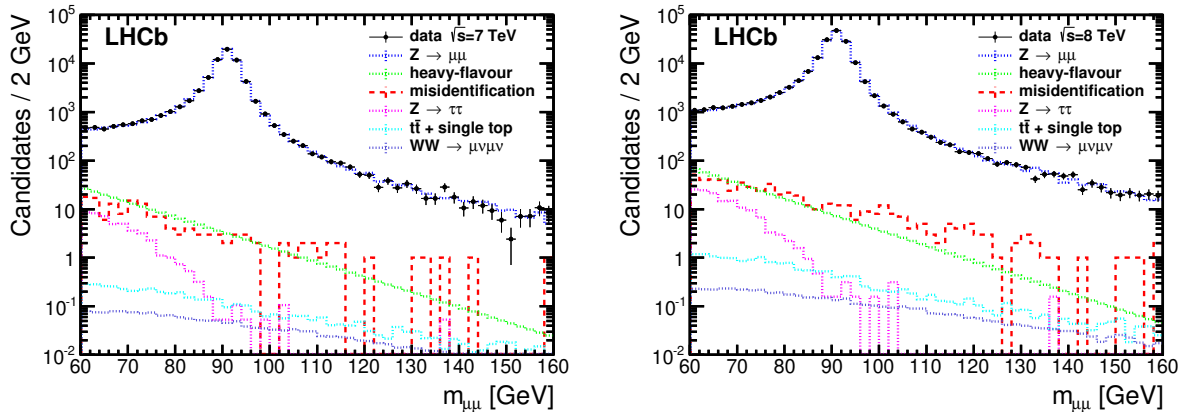


Figure 1: Dimuon invariant mass distribution for data, simulated signal and background processes for (left) $\sqrt{s} = 7$ TeV and (right) $\sqrt{s} = 8$ TeV.

4 Forward-backward asymmetry measurements

The forward-backward asymmetry is calculated from the selected dimuon candidates. Corrections are applied to account for efficiencies, biases in the reconstructed momenta of the muons and differences in resolution between simulation and data. Previous studies [20–22] have observed a dependence of trigger, track reconstruction and muon identification efficiencies on muon pseudorapidity. To account for this dependence, correction factors are evaluated from data using a tag-and-probe method [20] and applied to the measured forward-backward asymmetry.

The momentum measurement of a muon is sensitive both to uncertainties in the detector alignment and the magnetic field scale. The magnetic field scale has been calibrated using dimuon and other resonances at low mass and is known to a precision of 0.04% [9]. Low-mass resonances have also been used as input to the detector alignment, leading to a well-understood momentum calibration for low-momentum tracks [9, 23, 24]. However, studies for the analysis presented here, have revealed a small, but appreciable, dependence of the position of the Z resonance peak on muon kinematics. This effect can be attributed to residual detector misalignment. The corresponding muon curvature bias can be effectively parameterised in bins of the azimuthal angle of the muon about the beam axis. The parameters are determined using the difference between the Z mass peak in data and simulation. The procedure is applied separately to data collected at $\sqrt{s} = 7$ and 8 TeV, and for the two magnet polarities. The results are consistent with those presented in Ref. [21] in which a slightly different method was used.

To compare with theory predictions, the data are unfolded for acceptance and resolution effects. A Bayesian unfolding technique [25] is applied to the reconstructed dimuon invariant mass distribution [26]. The unfolding algorithm is trained on simulation by comparing the generated invariant mass to that after reconstruction. The simulation is corrected to have the same $m_{\mu\mu}$ resolution as observed in data. Finally, the data are corrected for background by subtracting the distribution for each background source determined as

Table 1: Weighted average of the absolute systematic uncertainties for A_{FB} , for different sources, given separately for $\sqrt{s} = 7$ and 8 TeV.

Source of uncertainty	$\sqrt{s} = 7$ TeV	$\sqrt{s} = 8$ TeV
curvature/momentum scale	0.0102	0.0050
data/simulation mass resolution	0.0032	0.0025
unfolding parameter	0.0033	0.0009
unfolding bias	0.0025	0.0025

described in Sec. 3. No correction is applied to the measured values of A_{FB} to account for the dilution due to imperfect knowledge of the initial quark direction, or to remove FSR effects. Instead, they are compared to predictions made within the same kinematic region and including FSR, as described in Sec. 5.

The following systematic uncertainties are considered when determining A_{FB} . The systematic uncertainty associated with the curvature correction is evaluated by varying these parameters within their uncertainty. The uncertainties on the calibration factors are dependent on the sample size, and are therefore larger for the $\sqrt{s} = 7$ TeV dataset. This is the largest source of systematic uncertainty. An uncertainty of $\pm 0.04\%$ is used for the momentum scale, determined from measurements of the magnetic field [9]. The bias in the unfolding procedure is determined from simulation by comparing unfolded samples with the generated true $m_{\mu\mu}$ distribution. An additional uncertainty to account for the dependence on the number of iterations used in the training of the unfolding algorithm is determined. This variation has a larger effect in regions where fewer events are simulated. The asymmetry of each background source does not vary significantly over the invariant mass range. An uncertainty of 10% is assigned to the background asymmetry, that covers the fluctuations observed in A_{FB} for each background source. The effect of the uncertainties in the efficiency corrections applied to the data is found to be negligible. The systematic uncertainties are determined separately for each bin of invariant mass and for both datasets. Their average values are summarized in Table 1.

The resulting measurements of A_{FB} for $\sqrt{s} = 7$ and 8 TeV data as a function of $m_{\mu\mu}$ are shown in Fig. 2 and tabulated in Tables 2 and 3.

5 Determination of $\sin^2\theta_{\text{W}}^{\text{eff}}$

The forward-backward asymmetry as a function of the dimuon invariant mass is compared with several sets of SM predictions generated with different values of $\sin^2\theta_{\text{W}}^{\text{eff}}$, denoted as $A_{\text{FB}}^{\text{pred}}$. The predictions are generated using POWHEG-BOX with $\sin^2\theta_{\text{W}}^{\text{eff}}$ values ranging from 0.22 to 0.24 for $\sqrt{s} = 7$ and 8 TeV, and the Z boson mass (M_Z) and the electromagnetic coupling constant (α_{EM}) fixed to the world average values [27]. The PDF set from

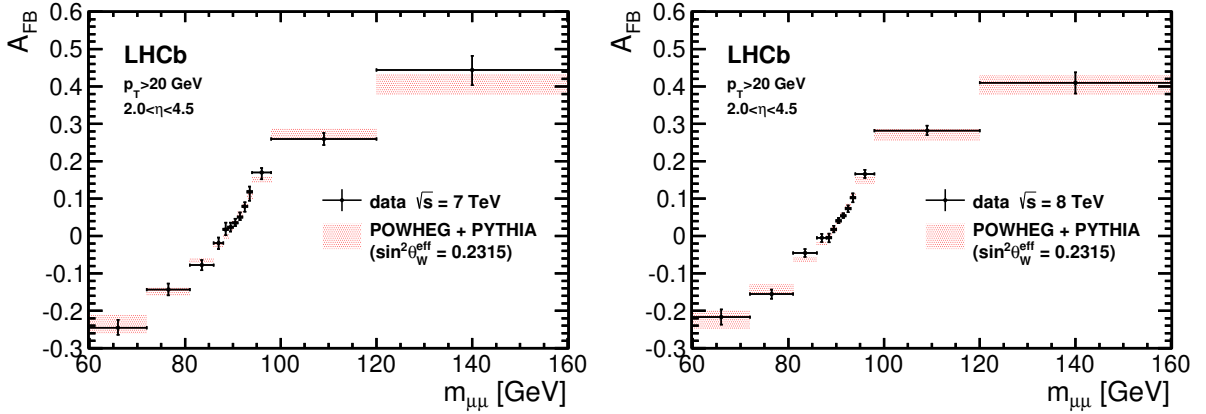


Figure 2: The measurements of A_{FB} as a function of the dimuon invariant mass for data compared to SM predictions for (left) $\sqrt{s} = 7$ TeV and (right) $\sqrt{s} = 8$ TeV. The SM predictions are calculated using POWHEG interfaced with PYTHIA for parton showering with the world average value for $\sin^2\theta_W^{\text{eff}} = 0.2315$ [27]. The data include both statistical and systematic uncertainties, and the SM predictions include the theoretical uncertainties described in Sec. 5.

NNPDF [28]³, with the strong coupling constant $\alpha_s(M_Z) = 0.118$, was used when generating the $A_{\text{FB}}^{\text{pred}}$ samples.

Theoretical uncertainties associated with the $A_{\text{FB}}^{\text{pred}}$ distributions are taken into account when determining $\sin^2\theta_W^{\text{eff}}$. They arise from the underlying PDF, the choice of renormalisation and factorisation scales, the value of α_s used, and the FSR calculation. Each of these uncertainties, referred to collectively as theoretical uncertainties, are obtained from simulation. The same uncertainty is assigned to $A_{\text{FB}}^{\text{pred}}$ at both $\sqrt{s} = 7$ and 8 TeV.

To estimate the theoretical uncertainty of the PDF set, one hundred replica samples are produced, each with a unique PDF set provided by NNPDF [29]. The value of $A_{\text{FB}}^{\text{pred}}$ is calculated as a function of $m_{\mu\mu}$ for each of these replicas, and the corresponding 68% confidence level interval determined. The size of this uncertainty is larger than the difference observed using CT10 [30] as an alternative PDF parameterisation.

Uncertainty in the PDFs affects $A_{\text{FB}}^{\text{pred}}$ in a way that is correlated across all dimuon invariant mass bins. The same systematic uncertainty is applied for both collision energies and is therefore fully correlated for the two samples.

The uncertainty due to the choice of renormalisation and factorisation scales is studied by varying them by a factor of 0.5 and 2 [31]. The uncertainty in the $\sin^2\theta_W^{\text{eff}}$ determination due to the uncertainty in α_s is estimated by studying the impact of a variation of ± 0.002 when generating samples using POWHEG-BOX. This covers the current uncertainty on α_s [27]. For both the α_s and scale uncertainties the final uncertainty is estimated by fitting a constant across the mass range to the maximum and minimum deviations in $A_{\text{FB}}^{\text{pred}}$ to minimise the effect of statistical fluctuations in the samples.

The uncertainty due to the implementation of FSR is treated as a theoretical un-

³NNPDF 2.3 QCD + QED NLO.

Table 2: Values for A_{FB} with the statistical and positive and negative systematic uncertainties for $\sqrt{s} = 7$ TeV data. The theoretical uncertainties presented in this table, corresponding to the PDF, scale and FSR uncertainties described in Sec. 5, affect only the predictions of A_{FB} and the $\sin^2\theta_{\text{W}}^{\text{eff}}$ determination, and do not apply to the uncertainties on the measured A_{FB} .

$m_{\mu\mu}(\text{GeV})$	A_{FB}	stat.	syst. +	syst. -	theoretical
60 – 72	-0.248	0.018	0.011	0.006	0.025
72 – 81	-0.144	0.015	0.006	0.003	0.011
81 – 86	-0.078	0.013	0.005	0.005	0.005
86 – 88	-0.017	0.013	0.007	0.009	0.005
88 – 89	0.016	0.013	0.012	0.008	0.005
89 – 90	0.023	0.010	0.006	0.006	0.005
90 – 91	0.033	0.008	0.007	0.004	0.005
91 – 92	0.047	0.008	0.009	0.002	0.005
92 – 93	0.082	0.010	0.004	0.010	0.006
93 – 94	0.127	0.014	0.004	0.016	0.009
94 – 98	0.175	0.012	0.003	0.014	0.009
98 – 120	0.259	0.015	0.007	0.006	0.014
120 – 160	0.451	0.037	0.004	0.017	0.026

certainty. It is obtained by comparing the $A_{\text{FB}}^{\text{pred}}$ from three different generators, FEWZ, Herwig++ and POWHEG-BOX+PYTHIA, before and after FSR. To be consistent with the POWHEG-BOX sample, the FEWZ generator is configured at NLO and electroweak corrections are not included. The maximum and minimum difference is then determined and used to estimate the systematic uncertainty associated with FSR. The average size of the separate theoretical uncertainties is summarised in Table 4, and the combined uncertainties as a function of invariant mass are given in Tables 2 and 3.

The $A_{\text{FB}}^{\text{pred}}$ shapes from POWHEG-BOX were cross-checked using the FEWZ generator at the same value of $\sin^2\theta_{\text{W}}^{\text{eff}}$ and the differences were found to be negligible.

The agreement between data and prediction is quantified by a χ^2 value defined as the square of the difference between the measured A_{FB} and $A_{\text{FB}}^{\text{pred}}$ divided by the quadratic sum of the statistical, systematic and theoretical uncertainties, taking into account the correlations in the uncertainties between the mass bins. A quadratic function is fitted to the χ^2 values of each set of fits as a function of $\sin^2\theta_{\text{W}}^{\text{eff}}$. The result is shown in Fig. 3. The value of $\sin^2\theta_{\text{W}}^{\text{eff}}$ at which χ^2 takes its minimum is quoted as the final result for the $\sin^2\theta_{\text{W}}^{\text{eff}}$ determination. The interval in $\sin^2\theta_{\text{W}}^{\text{eff}}$ corresponding to a variation of one unit in χ^2 is quoted as the uncertainty. The observed minimum values for the χ^2/ndf of the fit are 0.59 and 0.58, for the 7 and 8 TeV samples, respectively. The minima correspond to $\sin^2\theta_{\text{W}}^{\text{eff}} = 0.23219 \pm 0.00148$ and $\sin^2\theta_{\text{W}}^{\text{eff}} = 0.23074 \pm 0.00123$ respectively. Results are cross-checked using a set of pseudoexperiments with the same statistics and background fractions as those in data. The values of A_{FB} from the pseudoexperiments are fitted to the

Table 3: Values for A_{FB} with the statistical and positive and negative systematic uncertainties for $\sqrt{s} = 8$ TeV data. The theoretical uncertainties presented in this table, corresponding to the PDF, scale and FSR uncertainties described in Sec. 5, affect only the predictions of A_{FB} and the $\sin^2\theta_{\text{W}}^{\text{eff}}$ determination, and do not apply to the uncertainties on the measured A_{FB} .

$m_{\mu\mu}$ (GeV)	A_{FB}	stat.	syst. +	syst. -	theoretical
60 – 72	−0.217	0.014	0.015	0.014	0.025
72 – 81	−0.154	0.012	0.004	0.004	0.011
81 – 86	−0.046	0.010	0.003	0.002	0.005
86 – 88	−0.004	0.010	0.003	0.004	0.005
88 – 89	−0.002	0.011	0.003	0.007	0.005
89 – 90	0.016	0.008	0.006	0.002	0.005
90 – 91	0.040	0.006	0.005	0.003	0.005
91 – 92	0.053	0.006	0.004	0.002	0.005
92 – 93	0.075	0.008	0.004	0.006	0.006
93 – 94	0.104	0.011	0.003	0.006	0.009
94 – 98	0.166	0.010	0.005	0.006	0.009
98 – 120	0.280	0.012	0.006	0.002	0.014
120 – 160	0.412	0.027	0.005	0.009	0.026

Table 4: Weighted average of the absolute systematic uncertainties for $A_{\text{FB}}^{\text{pred}}$, for the different sources of theoretical uncertainty. The value quoted for the PDF uncertainty corresponds to the 68% confidence range, while for the others the maximum and minimum shifts are given. The correlations among the invariant mass bins are not taken into account.

Uncertainty	average $\Delta A_{\text{FB}}^{\text{pred}} $
PDF	0.0062
scale	0.0040
α_s	0.0030
FSR	0.0016

prediction, and the spread of the measured $\sin^2\theta_{\text{W}}^{\text{eff}}$ values agrees with the uncertainties in the values of the 7 and 8 TeV samples. A combination of these results, taking into account the correlation between systematic uncertainties for each centre-of-mass energy as well as the invariant mass bins, is obtained by calculating the full covariance matrix for the statistical, systematic and theoretical uncertainties. This yields

$$\sin^2\theta_{\text{W}}^{\text{eff}} = 0.23142 \pm 0.00073 \pm 0.00052 \pm 0.00056,$$

where the first uncertainty is statistical, the second systematic and the third theoretical.

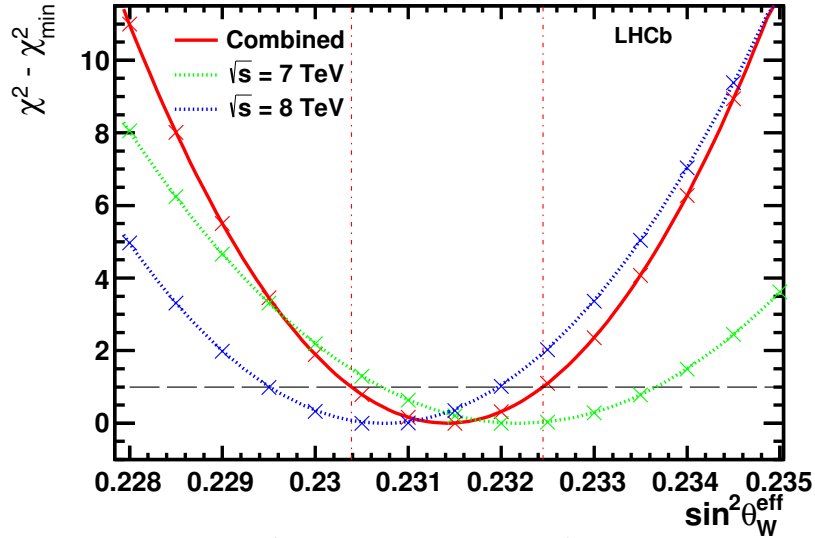


Figure 3: Difference between the χ^2 and the minimum χ^2 obtained by comparing the final $A_{\text{FB}}(m_{\mu\mu})$ measurements in data to $A_{\text{FB}}^{\text{pred}}$ calculated using values of $\sin^2 \theta_W^{\text{eff}}$ ranging from 0.22 to 0.24, indicated by the crosses on the plot. A quadratic fit is used to determine the minimum value for $\sin^2 \theta_W^{\text{eff}}$ and the corresponding uncertainty, and is shown for the different centre-of-mass energies and the combination. The black dashed horizontal line corresponds to one unit of χ^2 from the minimum and the intersecting $\sin^2 \theta_W^{\text{eff}}$ for the combination are indicated by the vertical red dashed lines.

A comparison between the $\sin^2 \theta_W^{\text{eff}}$ result obtained here and those from other experiments is shown in Fig. 4. The LHCb result agrees well with the world average and is one of the most precise measurements from hadron colliders.

6 Conclusions

The forward-backward asymmetry for the process $q\bar{q} \rightarrow Z \rightarrow \mu^+\mu^-$ as a function of the dimuon invariant mass is measured with the LHCb detector using proton proton collision data collected at centre-of-mass energies of $\sqrt{s} = 7$ and 8 TeV. The measurements are performed in the Collins-Soper frame, using muons with $p_T > 20$ GeV and $2.0 < \eta < 4.5$ with a combined invariant mass $60 < m_{\mu\mu} < 160$ GeV. The forward-backward asymmetry for each invariant mass bin is measured, together with the statistical and experimental uncertainties. The measurements at each centre-of-mass energy are used to determine a value for $\sin^2 \theta_W^{\text{eff}}$, by comparing to SM predictions that include FSR. The best fit values obtained are $\sin^2 \theta_W^{\text{eff}} = 0.23219 \pm 0.00148$ and $\sin^2 \theta_W^{\text{eff}} = 0.23074 \pm 0.00123$ for the two samples at $\sqrt{s} = 7$ and 8 TeV respectively. This leads to the combined result

$$\sin^2 \theta_W^{\text{eff}} = 0.23142 \pm 0.00073 \pm 0.00052 \pm 0.00056,$$

where the first uncertainty is statistical, the second systematic and the third theoretical.

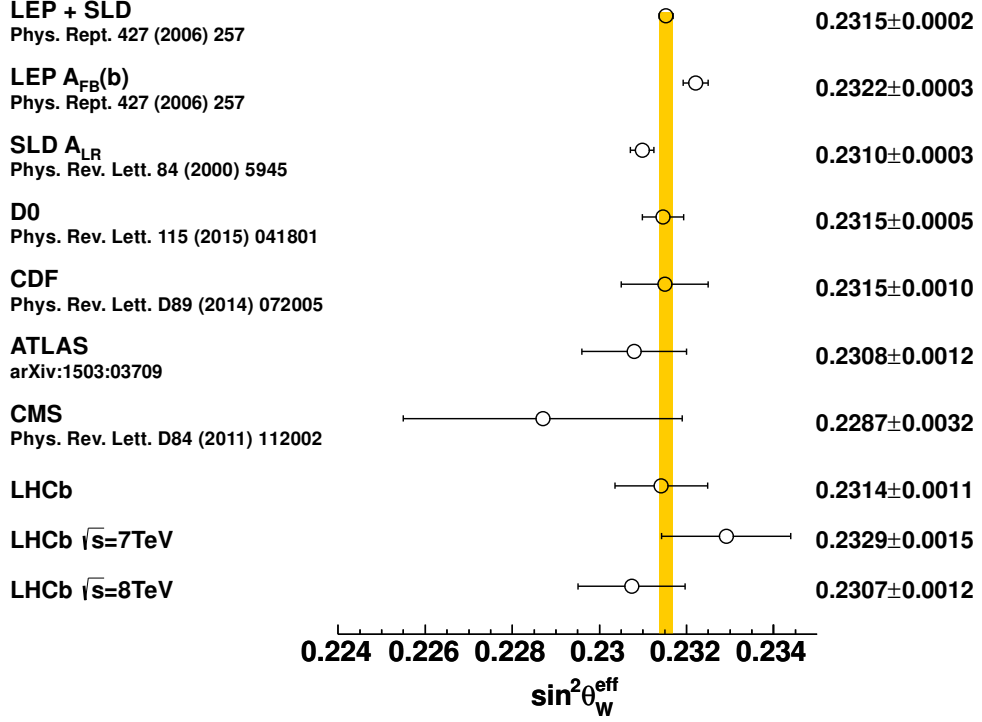


Figure 4: A comparison of the $\sin^2\theta_W^{\text{eff}}$ measurement at LHCb and other experiments. The combined LEP and SLD measurement is indicated by the vertical yellow band.

The measurement of $\sin^2\theta_W^{\text{eff}}$ presented here agrees with previous measurements. The uncertainty from the PDF is the dominant theoretical uncertainty. Further high precision measurements at the LHC are expected to provide additional constraints in the forward region and reduce this uncertainty. As the size of the data sample increases, it will become possible to perform a measurement of A_{FB} double-differentially in dimuon invariant mass and rapidity. Such an approach will allow the analysis to take further advantage of the increased sensitivity of A_{FB} to $\sin^2\theta_W^{\text{eff}}$ in the most forward region.

Acknowledgements

We express our gratitude to our colleagues in the CERN accelerator departments for the excellent performance of the LHC. We thank the technical and administrative staff at the LHCb institutes. We acknowledge support from CERN and from the national agencies: CAPES, CNPq, FAPERJ and FINEP (Brazil); NSFC (China); CNRS/IN2P3 (France); BMBF, DFG and MPG (Germany); INFN (Italy); FOM and NWO (The Netherlands); MNiSW and NCN (Poland); MEN/IFA (Romania); MinES and FANO (Russia); MinECo (Spain); SNSF and SER (Switzerland); NASU (Ukraine); STFC (United Kingdom); NSF (USA). We acknowledge the computing resources that are provided by CERN, IN2P3 (France), KIT and DESY (Germany), INFN (Italy), SURF (The Netherlands), PIC

(Spain), GridPP (United Kingdom), RRCKI (Russia), CSCS (Switzerland), IFIN-HH (Romania), CBPF (Brazil), PL-GRID (Poland) and OSC (USA). We are indebted to the communities behind the multiple open source software packages on which we depend. We are also thankful for the computing resources and the access to software R&D tools provided by Yandex LLC (Russia). Individual groups or members have received support from AvH Foundation (Germany), EPLANET, Marie Skłodowska-Curie Actions and ERC (European Union), Conseil Général de Haute-Savoie, Labex ENIGMASS and OCEVU, Région Auvergne (France), RFBR (Russia), XuntaGal and GENCAT (Spain), The Royal Society and Royal Commission for the Exhibition of 1851 (United Kingdom).

References

- [1] ALEPH collaboration, DELPHI collaboration, L3 collaboration, OPAL collaboration, SLD collaboration, LEP Electroweak Working Group, SLD Electroweak Group, SLD Heavy Flavour Group, S. Schael *et al.*, *Precision electroweak measurements on the Z resonance*, Phys. Rept. **427** (2006) 257, [arXiv:hep-ex/0509008](#).
- [2] J. Collins and D. Soper, *Angular distribution of dileptons in high-energy hadron collisions*, Phys. Rev. D **16** (1977) 2219.
- [3] SLD collaboration, K. Abe *et al.*, *A high-precision measurement of the left-right Z boson cross-section asymmetry*, Phys. Rev. Lett. **84** (2000) 5945.
- [4] CDF collaboration, T. A. Aaltonen *et al.*, *Indirect measurement of $\sin^2 \theta_W$ (or M_W) using $\mu^+ \mu^-$ pairs from γ^*/Z bosons produced in $p\bar{p}$ collisions at a center-of-momentum energy of 1.96 TeV*, Phys. Rev. **D89** (2014) 072005, [arXiv:1402.2239](#).
- [5] D0 collaboration, V. M. Abazov *et al.*, *Measurement of the effective weak mixing angle in $p\bar{p} \rightarrow Z/\gamma^* \rightarrow e^+ e^-$ events*, Phys. Rev. Lett. **115** (2015) 041801, [arXiv:1408.5016](#).
- [6] ATLAS collaboration, G. Aad *et al.*, *Measurement of the forward-backward asymmetry of electron and muon pair-production in pp collisions at $\sqrt{s} = 7$ TeV with the ATLAS detector*, [arXiv:1503.03709](#).
- [7] CMS collaboration, S. Chatrchyan *et al.*, *Measurement of the weak mixing angle with the Drell-Yan process in proton-proton collisions at the LHC*, Phys. Rev. **D84** (2011) 112002, [arXiv:1110.2682](#).
- [8] LHCb collaboration, A. A. Alves Jr. *et al.*, *The LHCb detector at the LHC*, JINST **3** (2008) S08005.
- [9] LHCb collaboration, R. Aaij *et al.*, *LHCb detector performance*, Int. J. Mod. Phys. **A30** (2015) 1530022, [arXiv:1412.6352](#).
- [10] T. Sjöstrand, S. Mrenna, and P. Skands, *PYTHIA 6.4 physics and manual*, JHEP **05** (2006) 026, [arXiv:hep-ph/0603175](#).

- [11] T. Sjöstrand, S. Mrenna, and P. Z. Skands, *A brief introduction to PYTHIA 8.1*, Comput. Phys. Commun. **178** (2008) 852, [arXiv:0710.3820](#).
- [12] I. Belyaev *et al.*, *Handling of the generation of primary events in Gauss, the LHCb simulation framework*, J. Phys. Conf. Ser. **331** (2011) 032047.
- [13] D. J. Lange, *The EvtGen particle decay simulation package*, Nucl. Instrum. Meth. **A462** (2001) 152.
- [14] P. Golonka and Z. Was, *PHOTOS Monte Carlo: A precision tool for QED corrections in Z and W decays*, Eur. Phys. J. **C45** (2006) 97, [arXiv:hep-ph/0506026](#).
- [15] Geant4 collaboration, J. Allison *et al.*, *Geant4 developments and applications*, IEEE Trans. Nucl. Sci. **53** (2006) 270.
- [16] M. Clemencic *et al.*, *The LHCb simulation application, Gauss: Design, evolution and experience*, J. Phys. Conf. Ser. **331** (2011) 032023.
- [17] S. Alioli, P. Nason, C. Oleari, and E. Re, *NLO vector-boson production matched with shower in POWHEG*, JHEP **07** (2008) 060, [arXiv:0805.4802](#).
- [18] M. Bahr *et al.*, *Herwig++ physics and manual*, Eur. Phys. J. **C58** (2008) 639, [arXiv:0803.0883](#).
- [19] R. Gavin, Y. Li, F. Petriello, and S. Quackenbush, *FEWZ 2.0: A code for hadronic Z production at next-to-next-to-leading order*, Comput. Phys. Commun. **182** (2011) 2388, [arXiv:1011.3540](#).
- [20] LHCb collaboration, R. Aaij *et al.*, *Measurement of the forward Z boson production cross-section in pp collisions at $\sqrt{s} = 7$ TeV*, JHEP **08** (2015) 039, [arXiv:1505.07024](#).
- [21] LHCb collaboration, R. Aaij *et al.*, *Measurement of the forward W boson cross-section in pp collisions at $\sqrt{s} = 7$ TeV*, JHEP **12** (2014) 079, [arXiv:1408.4354](#).
- [22] LHCb collaboration, R. Aaij *et al.*, *Inclusive W and Z production in the forward region at $\sqrt{s} = 7$ TeV*, JHEP **06** (2012) 058, [arXiv:1204.1620](#).
- [23] J. Amoraal *et al.*, *Application of vertex and mass constraints in track-based alignment*, Nucl. Instrum. Meth. **A712** (2013) 48, [arXiv:1207.4756](#).
- [24] LHCb collaboration, R. Aaij *et al.*, *Measurements of the Λ_b^0 , Ξ_b^- , and Ω_b^- baryon masses*, Phys. Rev. Lett. **110** (2013) 182001, [arXiv:1302.1072](#).
- [25] G. D’Agostini, *A multidimensional unfolding method based on Bayes’ theorem*, Nucl. Instrum. Meth. **A362** (1995) 487.
- [26] T. Adye, *Unfolding algorithms and tests using RooUnfold*, in *Proceedings of the PHYSTAT 2011 workshop, CERN, Geneva, Switzerland, January 2011, CERN-2011-006, pp 313-318*, pp. 313–318, 2011. [arXiv:1105.1160](#).

- [27] Particle Data Group, K. A. Olive *et al.*, *Review of particle physics*, Chin. Phys. **C38** (2014) 090001.
- [28] NNPDF collaboration, R. D. Ball *et al.*, *Parton distributions with LHC data*, Nucl. Phys. **B867** (2013) 244, [arXiv:1207.1303](#).
- [29] NNPDF collaboration, R. D. Ball *et al.*, *Parton distributions with QED corrections*, Nucl. Phys. **B877** (2013) 290, [arXiv:1308.0598](#).
- [30] H.-L. Lai *et al.*, *New parton distributions for collider physics*, Phys. Rev. **D82** (2010) 074024, [arXiv:1007.2241](#).
- [31] K. Hamilton, P. Nason, E. Re, and G. Zanderighi, *NNLOPS simulation of Higgs boson production*, JHEP **10** (2013) 222, [arXiv:1309.0017](#).

LHCb collaboration

R. Aaij³⁸, B. Adeva³⁷, M. Adinolfi⁴⁶, A. Affolder⁵², Z. Ajaltouni⁵, S. Akar⁶, J. Albrecht⁹, F. Alessio³⁸, M. Alexander⁵¹, S. Ali⁴¹, G. Alkhazov³⁰, P. Alvarez Cartelle⁵³, A.A. Alves Jr⁵⁷, S. Amato², S. Amerio²², Y. Amhis⁷, L. An³, L. Anderlini¹⁷, J. Anderson⁴⁰, G. Andreassi³⁹, M. Andreotti^{16,f}, J.E. Andrews⁵⁸, R.B. Appleby⁵⁴, O. Aquines Gutierrez¹⁰, F. Archilli³⁸, P. d'Argent¹¹, A. Artamonov³⁵, M. Artuso⁵⁹, E. Aslanides⁶, G. Auriemma^{25,m}, M. Baalouch⁵, S. Bachmann¹¹, J.J. Back⁴⁸, A. Badalov³⁶, C. Baesso⁶⁰, W. Baldini^{16,38}, R.J. Barlow⁵⁴, C. Barschel³⁸, S. Barsuk⁷, W. Barter³⁸, V. Batozskaya²⁸, V. Battista³⁹, A. Bay³⁹, L. Beaucourt⁴, J. Beddow⁵¹, F. Bedeschi²³, I. Bediaga¹, L.J. Bel⁴¹, V. Bellec³⁹, N. Belloli^{20,j}, I. Belyaev³¹, E. Ben-Haim⁸, G. Bencivenni¹⁸, S. Benson³⁸, J. Benton⁴⁶, A. Berezhnoy³², R. Bernet⁴⁰, A. Bertolin²², M.-O. Bettler³⁸, M. van Beuzekom⁴¹, A. Bien¹¹, S. Bifani⁴⁵, P. Billoir⁸, T. Bird⁵⁴, A. Birnkraut⁹, A. Bizzeti^{17,h}, T. Blake⁴⁸, F. Blanc³⁹, J. Blouw¹⁰, S. Blusk⁵⁹, V. Bocci²⁵, A. Bondar³⁴, N. Bondar^{30,38}, W. Bonivento¹⁵, S. Borghi⁵⁴, M. Borsato⁷, T.J.V. Bowcock⁵², E. Bowen⁴⁰, C. Bozzi¹⁶, S. Braun¹¹, M. Britsch¹⁰, T. Britton⁵⁹, J. Brodzicka⁵⁴, N.H. Brook⁴⁶, E. Buchanan⁴⁶, A. Bursche⁴⁰, J. Buytaert³⁸, S. Cadeddu¹⁵, R. Calabrese^{16,f}, M. Calvi^{20,j}, M. Calvo Gomez^{36,o}, P. Campana¹⁸, D. Campora Perez³⁸, L. Capriotti⁵⁴, A. Carbone^{14,d}, G. Carboni^{24,k}, R. Cardinale^{19,i}, A. Cardini¹⁵, P. Carniti^{20,j}, L. Carson⁵⁰, K. Carvalho Akiba^{2,38}, G. Casse⁵², L. Cassina^{20,j}, L. Castillo Garcia³⁸, M. Cattaneo³⁸, Ch. Cauet⁹, G. Cavallero¹⁹, R. Cenci^{23,s}, M. Charles⁸, Ph. Charpentier³⁸, M. Chefdeville⁴, S. Chen⁵⁴, S.-F. Cheung⁵⁵, N. Chiapolini⁴⁰, M. Chrzasczcz⁴⁰, X. Cid Vidal³⁸, G. Ciezarek⁴¹, P.E.L. Clarke⁵⁰, M. Clemencic³⁸, H.V. Cliff⁴⁷, J. Closier³⁸, V. Coco³⁸, J. Cogan⁶, E. Cogneras⁵, V. Cogoni^{15,e}, L. Cojocariu²⁹, G. Collazuol²², P. Collins³⁸, A. Comerma-Montells¹¹, A. Contu¹⁵, A. Cook⁴⁶, M. Coombes⁴⁶, S. Coquereau⁸, G. Corti³⁸, M. Corvo^{16,f}, B. Couturier³⁸, G.A. Cowan⁵⁰, D.C. Craik⁴⁸, A. Crocombe⁴⁸, M. Cruz Torres⁶⁰, S. Cunliffe⁵³, R. Currie⁵³, C. D'Ambrosio³⁸, E. Dall'Occo⁴¹, J. Dalseno⁴⁶, P.N.Y. David⁴¹, A. Davis⁵⁷, O. De Aguiar Francisco², K. De Bruyn⁶, S. De Capua⁵⁴, M. De Cian¹¹, J.M. De Miranda¹, L. De Paula², P. De Simone¹⁸, C.-T. Dean⁵¹, D. Decamp⁴, M. Deckenhoff⁹, L. Del Buono⁸, N. Déléage⁴, M. Demmer⁹, D. Derkach⁶⁵, O. Deschamps⁵, F. Dettori³⁸, B. Dey²¹, A. Di Canto³⁸, F. Di Ruscio²⁴, H. Dijkstra³⁸, S. Donleavy⁵², F. Dordei¹¹, M. Dorigo³⁹, A. Dosil Suárez³⁷, D. Dossett⁴⁸, A. Dovbnya⁴³, K. Dreimanis⁵², L. Dufour⁴¹, G. Dujany⁵⁴, F. Dupertuis³⁹, P. Durante³⁸, R. Dzhelezhyan³⁵, A. Dziurda²⁶, A. Dzyuba³⁰, S. Easo^{49,38}, U. Egede⁵³, V. Egorychev³¹, S. Eidelman³⁴, S. Eisenhardt⁵⁰, U. Eitschberger⁹, R. Ekelhof⁹, L. Eklund⁵¹, I. El Rifai⁵, Ch. Elsasser⁴⁰, S. Ely⁵⁹, S. Esen¹¹, H.M. Evans⁴⁷, T. Evans⁵⁵, A. Falabella¹⁴, C. Färber³⁸, N. Farley⁴⁵, S. Farry⁵², R. Fay⁵², D. Ferguson⁵⁰, V. Fernandez Albor³⁷, F. Ferrari¹⁴, F. Ferreira Rodrigues¹, M. Ferro-Luzzi³⁸, S. Filippov³³, M. Fiore^{16,38,f}, M. Fiorini^{16,f}, M. Firlej²⁷, C. Fitzpatrick³⁹, T. Fiutowski²⁷, K. Fohl³⁸, P. Fol⁵³, M. Fontana¹⁵, F. Fontanelli^{19,i}, R. Forty³⁸, M. Frank³⁸, C. Frei³⁸, M. Frosini¹⁷, J. Fu²¹, E. Furfaro^{24,k}, A. Gallas Torreira³⁷, D. Galli^{14,d}, S. Gallorini²², S. Gambetta⁵⁰, M. Gandelman², P. Gandini⁵⁵, Y. Gao³, J. García Pardiñas³⁷, J. Garra Tico⁴⁷, L. Garrido³⁶, D. Gascon³⁶, C. Gaspar³⁸, R. Gauld⁵⁵, L. Gavardi⁹, G. Gazzoni⁵, D. Gerick¹¹, E. Gersabeck¹¹, M. Gersabeck⁵⁴, T. Gershon⁴⁸, Ph. Ghez⁴, S. Gianì³⁹, V. Gibson⁴⁷, O.G. Girard³⁹, L. Giubega²⁹, V.V. Gligorov³⁸, C. Göbel⁶⁰, D. Golubkov³¹, A. Golutvin^{53,38}, A. Gomes^{1,a}, C. Gotti^{20,j}, M. Grabalosa Gándara⁵, R. Graciani Diaz³⁶, L.A. Granado Cardoso³⁸, E. Graugés³⁶, E. Graverini⁴⁰, G. Graziani¹⁷, A. Grecu²⁹, E. Greening⁵⁵, S. Gregson⁴⁷, P. Griffith⁴⁵, L. Grillo¹¹, O. Grünberg⁶³, B. Gui⁵⁹, E. Gushchin³³, Yu. Guz^{35,38}, T. Gys³⁸, T. Hadavizadeh⁵⁵, C. Hadjivasiliou⁵⁹, G. Haefeli³⁹, C. Haen³⁸, S.C. Haines⁴⁷, S. Hall⁵³,

B. Hamilton⁵⁸, X. Han¹¹, S. Hansmann-Menzemer¹¹, N. Harnew⁵⁵, S.T. Harnew⁴⁶, J. Harrison⁵⁴,
 J. He³⁸, T. Head³⁹, V. Heijne⁴¹, K. Hennessy⁵², P. Henrard⁵, L. Henry⁸, E. van Herwijnen³⁸,
 M. Heß⁶³, A. Hicheur², D. Hill⁵⁵, M. Hoballah⁵, C. Hombach⁵⁴, W. Hulsbergen⁴¹, T. Humair⁵³,
 N. Hussain⁵⁵, D. Hutchcroft⁵², D. Hynds⁵¹, M. Idzik²⁷, P. Ilten⁵⁶, R. Jacobsson³⁸, A. Jaeger¹¹,
 J. Jalocha⁵⁵, E. Jans⁴¹, A. Jawahery⁵⁸, F. Jing³, M. John⁵⁵, D. Johnson³⁸, C.R. Jones⁴⁷,
 C. Joram³⁸, B. Jost³⁸, N. Jurik⁵⁹, S. Kandybei⁴³, W. Kanso⁶, M. Karacson³⁸, T.M. Karbach^{38,†},
 S. Karodia⁵¹, M. Kecke¹¹, M. Kelsey⁵⁹, I.R. Kenyon⁴⁵, M. Kenzie³⁸, T. Ketel⁴², E. Khairullin⁶⁵,
 B. Khanji^{20,38,j}, C. Khurewathanakul³⁹, S. Klaver⁵⁴, K. Klimaszewski²⁸, O. Kochebina⁷,
 M. Kolpin¹¹, I. Komarov³⁹, R.F. Koopman⁴², P. Koppenburg^{41,38}, M. Kozeiha⁵, L. Kravchuk³³,
 K. Kreplin¹¹, M. Kreps⁴⁸, G. Krocker¹¹, P. Krokovny³⁴, F. Kruse⁹, W. Krzemien²⁸,
 W. Kucewicz^{26,n}, M. Kucharczyk²⁶, V. Kudryavtsev³⁴, A. K. Kuonen³⁹, K. Kurek²⁸,
 T. Kvaratskheliya³¹, D. Lacarrere³⁸, G. Lafferty⁵⁴, A. Lai¹⁵, D. Lambert⁵⁰, G. Lanfranchi¹⁸,
 C. Langenbruch⁴⁸, B. Langhans³⁸, T. Latham⁴⁸, C. Lazzeroni⁴⁵, R. Le Gac⁶, J. van Leerdam⁴¹,
 J.-P. Lees⁴, R. Lefèvre⁵, A. Leflat^{32,38}, J. Lefrançois⁷, E. Lemos Cid³⁷, O. Leroy⁶, T. Lesiak²⁶,
 B. Leverington¹¹, Y. Li⁷, T. Likhomanenko^{65,64}, M. Liles⁵², R. Lindner³⁸, C. Linn³⁸,
 F. Lionetto⁴⁰, B. Liu¹⁵, X. Liu³, D. Loh⁴⁸, I. Longstaff⁵¹, J.H. Lopes², D. Lucchesi^{22,q},
 M. Lucio Martinez³⁷, H. Luo⁵⁰, A. Lupato²², E. Luppi^{16,f}, O. Lupton⁵⁵, A. Lusiani²³,
 F. Machefert⁷, F. Maciuc²⁹, O. Maev³⁰, K. Maguire⁵⁴, S. Malde⁵⁵, A. Malinin⁶⁴, G. Manca⁷,
 G. Mancinelli⁶, P. Manning⁵⁹, A. Mapelli³⁸, J. Maratas⁵, J.F. Marchand⁴, U. Marconi¹⁴,
 C. Marin Benito³⁶, P. Marino^{23,38,s}, J. Marks¹¹, G. Martellotti²⁵, M. Martin⁶, M. Martinelli³⁹,
 D. Martinez Santos³⁷, F. Martinez Vidal⁶⁶, D. Martins Tostes², A. Massafferri¹, R. Matev³⁸,
 A. Mathad⁴⁸, Z. Mathe³⁸, C. Matteuzzi²⁰, A. Mauri⁴⁰, B. Maurin³⁹, A. Mazurov⁴⁵,
 M. McCann⁵³, J. McCarthy⁴⁵, A. McNab⁵⁴, R. McNulty¹², B. Meadows⁵⁷, F. Meier⁹,
 M. Meissner¹¹, D. Melnychuk²⁸, M. Merk⁴¹, E. Michielin²², D.A. Milanese⁶², M.-N. Minard⁴,
 D.S. Mitzel¹¹, J. Molina Rodriguez⁶⁰, I.A. Monroy⁶², S. Monteil⁵, M. Morandin²²,
 P. Morawski²⁷, A. Mordà⁶, M.J. Morello^{23,s}, J. Moron²⁷, A.B. Morris⁵⁰, R. Mountain⁵⁹,
 F. Muheim⁵⁰, D. Müller⁵⁴, J. Müller⁹, K. Müller⁴⁰, V. Müller⁹, M. Mussini¹⁴, B. Muster³⁹,
 P. Naik⁴⁶, T. Nakada³⁹, R. Nandakumar⁴⁹, A. Nandi⁵⁵, I. Nasteva², M. Needham⁵⁰, N. Neri²¹,
 S. Neubert¹¹, N. Neufeld³⁸, M. Neuner¹¹, A.D. Nguyen³⁹, T.D. Nguyen³⁹, C. Nguyen-Mau^{39,p},
 V. Niess⁵, R. Niet⁹, N. Nikitin³², T. Nikodem¹¹, A. Novoselov³⁵, D.P. O’Hanlon⁴⁸,
 A. Oblakowska-Mucha²⁷, V. Obraztsov³⁵, S. Ogilvy⁵¹, O. Okhrimenko⁴⁴, R. Oldeman^{15,e},
 C.J.G. Onderwater⁶⁷, B. Osorio Rodrigues¹, J.M. Otalora Goicochea², A. Otto³⁸, P. Owen⁵³,
 A. Oyanguren⁶⁶, A. Palano^{13,c}, F. Palombo^{21,t}, M. Palutan¹⁸, J. Panman³⁸, A. Papanestis⁴⁹,
 M. Pappagallo⁵¹, L.L. Pappalardo^{16,f}, C. Pappenheimer⁵⁷, W. Parker⁵⁸, C. Parkes⁵⁴,
 G. Passaleva¹⁷, G.D. Patel⁵², M. Patel⁵³, C. Patrignani^{19,i}, A. Pearce^{54,49}, A. Pellegrino⁴¹,
 G. Penso^{25,l}, M. Pepe Altarelli³⁸, S. Perazzini^{14,d}, P. Perret⁵, L. Pescatore⁴⁵, K. Petridis⁴⁶,
 A. Petrolini^{19,i}, M. Petruzzio²¹, E. Picatoste Olloqui³⁶, B. Pietrzyk⁴, T. Pilar⁴⁸, D. Pinci²⁵,
 A. Pistone¹⁹, A. Piucci¹¹, S. Playfer⁵⁰, M. Plo Casasus³⁷, T. Poikela³⁸, F. Polci⁸,
 A. Poluektov^{48,34}, I. Polyakov³¹, E. Polcarpo², A. Popov³⁵, D. Popov^{10,38}, B. Popovici²⁹,
 C. Potterat², E. Price⁴⁶, J.D. Price⁵², J. Prisciandaro³⁷, A. Pritchard⁵², C. Prouve⁴⁶,
 V. Pugatch⁴⁴, A. Puig Navarro³⁹, G. Punzi^{23,r}, W. Qian⁴, R. Quagliani^{7,46}, B. Rachwal²⁶,
 J.H. Rademacker⁴⁶, M. Rama²³, M.S. Rangel², I. Raniuk⁴³, N. Rauschmayr³⁸, G. Raven⁴²,
 F. Redi⁵³, S. Reichert⁵⁴, M.M. Reid⁴⁸, A.C. dos Reis¹, S. Ricciardi⁴⁹, S. Richards⁴⁶, M. Rihl³⁸,
 K. Rinnert⁵², V. Rives Molina³⁶, P. Robbe^{7,38}, A.B. Rodrigues¹, E. Rodrigues⁵⁴,
 J.A. Rodriguez Lopez⁶², P. Rodriguez Perez⁵⁴, S. Roiser³⁸, V. Romanovsky³⁵,
 A. Romero Vidal³⁷, J. W. Ronayne¹², M. Rotondo²², J. Rouvinet³⁹, T. Ruf³⁸, P. Ruiz Valls⁶⁶,

J.J. Saborido Silva³⁷, N. Sagidova³⁰, P. Sail⁵¹, B. Saitta^{15,e}, V. Salustino Guimaraes²,
C. Sanchez Mayordomo⁶⁶, B. Sanmartin Sedes³⁷, R. Santacesaria²⁵, C. Santamarina Rios³⁷,
M. Santimaria¹⁸, E. Santovetti^{24,k}, A. Sarti^{18,l}, C. Satriano^{25,m}, A. Satta²⁴, D.M. Saunders⁴⁶,
D. Savrina^{31,32}, M. Schiller³⁸, H. Schindler³⁸, M. Schlupp⁹, M. Schmelling¹⁰, T. Schmelzer⁹,
B. Schmidt³⁸, O. Schneider³⁹, A. Schopper³⁸, M. Schubiger³⁹, M.-H. Schune⁷, R. Schwemmer³⁸,
B. Sciascia¹⁸, A. Sciubba^{25,l}, A. Semennikov³¹, N. Serra⁴⁰, J. Serrano⁶, L. Sestini²², P. Seyfert²⁰,
M. Shapkin³⁵, I. Shapoval^{16,43,f}, Y. Shcheglov³⁰, T. Shears⁵², L. Shekhtman³⁴, V. Shevchenko⁶⁴,
A. Shires⁹, B.G. Siddi¹⁶, R. Silva Coutinho^{48,40}, L. Silva de Oliveira², G. Simi²², M. Sirendi⁴⁷,
N. Skidmore⁴⁶, T. Skwarnicki⁵⁹, E. Smith^{55,49}, E. Smith⁵³, I.T. Smith⁵⁰, J. Smith⁴⁷, M. Smith⁵⁴,
H. Snoek⁴¹, M.D. Sokoloff^{57,38}, F.J.P. Soler⁵¹, F. Soomro³⁹, D. Souza⁴⁶, B. Souza De Paula²,
B. Spaan⁹, P. Spradlin⁵¹, S. Sridharan³⁸, F. Stagni³⁸, M. Stahl¹¹, S. Stahl³⁸, S. Stefkova⁵³,
O. Steinkamp⁴⁰, O. Stenyakin³⁵, S. Stevenson⁵⁵, S. Stoica²⁹, S. Stone⁵⁹, B. Storaci⁴⁰,
S. Stracka^{23,s}, M. Straticiu²⁹, U. Straumann⁴⁰, L. Sun⁵⁷, W. Sutcliffe⁵³, K. Swientek²⁷,
S. Swientek⁹, V. Syropoulos⁴², M. Szczekowski²⁸, T. Szumlak²⁷, S. T'Jampens⁴, A. Tayduganov⁶,
T. Tekampe⁹, M. Teklishyn⁷, G. Tellarini^{16,f}, F. Teubert³⁸, C. Thomas⁵⁵, E. Thomas³⁸,
J. van Tilburg⁴¹, V. Tisserand⁴, M. Tobin³⁹, J. Todd⁵⁷, S. Tolk⁴², L. Tomassetti^{16,f}, D. Tonelli³⁸,
S. Topp-Joergensen⁵⁵, N. Tori⁵⁵, E. Tournefier⁴, S. Tourneur³⁹, K. Trabelsi³⁹, M.T. Tran³⁹,
M. Tresch⁴⁰, A. Trisovic³⁸, A. Tsaregorodtsev⁶, P. Tsopelas⁴¹, N. Tuning^{41,38}, A. Ukleja²⁸,
A. Ustyuzhanin^{65,64}, U. Uwer¹¹, C. Vacca^{15,e}, V. Vagnoni¹⁴, G. Valenti¹⁴, A. Vallier⁷,
R. Vazquez Gomez¹⁸, P. Vazquez Regueiro³⁷, C. Vázquez Sierra³⁷, S. Vecchi¹⁶, J.J. Velthuis⁴⁶,
M. Veltri^{17,g}, G. Veneziano³⁹, M. Vesterinen¹¹, B. Viaud⁷, D. Vieira², M. Vieites Diaz³⁷,
X. Vilasis-Cardona^{36,o}, V. Volkov³², A. Vollhardt⁴⁰, D. Volyansky¹⁰, D. Voong⁴⁶,
A. Vorobyev³⁰, V. Vorobyev³⁴, C. Voß⁶³, J.A. de Vries⁴¹, R. Waldi⁶³, C. Wallace⁴⁸, R. Wallace¹²,
J. Walsh²³, S. Wandernoth¹¹, J. Wang⁵⁹, D.R. Ward⁴⁷, N.K. Watson⁴⁵, D. Websdale⁵³,
A. Weiden⁴⁰, M. Whitehead⁴⁸, G. Wilkinson^{55,38}, M. Wilkinson⁵⁹, M. Williams³⁸,
M.P. Williams⁴⁵, M. Williams⁵⁶, T. Williams⁴⁵, F.F. Wilson⁴⁹, J. Wimberley⁵⁸, J. Wishahi⁹,
W. Wislicki²⁸, M. Witek²⁶, G. Wormser⁷, S.A. Wotton⁴⁷, S. Wright⁴⁷, K. Wyllie³⁸, Y. Xie⁶¹,
Z. Xu³⁹, Z. Yang³, J. Yu⁶¹, X. Yuan³⁴, O. Yushchenko³⁵, M. Zangoli¹⁴, M. Zavertyaev^{10,b},
L. Zhang³, Y. Zhang³, A. Zhelezov¹¹, A. Zhokhov³¹, L. Zhong³, S. Zucchelli¹⁴.

¹ Centro Brasileiro de Pesquisas Físicas (CBPF), Rio de Janeiro, Brazil

² Universidade Federal do Rio de Janeiro (UFRJ), Rio de Janeiro, Brazil

³ Center for High Energy Physics, Tsinghua University, Beijing, China

⁴ LAPP, Université Savoie Mont-Blanc, CNRS/IN2P3, Annecy-Le-Vieux, France

⁵ Clermont Université, Université Blaise Pascal, CNRS/IN2P3, LPC, Clermont-Ferrand, France

⁶ CPPM, Aix-Marseille Université, CNRS/IN2P3, Marseille, France

⁷ LAL, Université Paris-Sud, CNRS/IN2P3, Orsay, France

⁸ LPNHE, Université Pierre et Marie Curie, Université Paris Diderot, CNRS/IN2P3, Paris, France

⁹ Fakultät Physik, Technische Universität Dortmund, Dortmund, Germany

¹⁰ Max-Planck-Institut für Kernphysik (MPIK), Heidelberg, Germany

¹¹ Physikalisches Institut, Ruprecht-Karls-Universität Heidelberg, Heidelberg, Germany

¹² School of Physics, University College Dublin, Dublin, Ireland

¹³ Sezione INFN di Bari, Bari, Italy

¹⁴ Sezione INFN di Bologna, Bologna, Italy

¹⁵ Sezione INFN di Cagliari, Cagliari, Italy

¹⁶ Sezione INFN di Ferrara, Ferrara, Italy

¹⁷ Sezione INFN di Firenze, Firenze, Italy

¹⁸ Laboratori Nazionali dell'INFN di Frascati, Frascati, Italy

- ¹⁹ *Sezione INFN di Genova, Genova, Italy*
- ²⁰ *Sezione INFN di Milano Bicocca, Milano, Italy*
- ²¹ *Sezione INFN di Milano, Milano, Italy*
- ²² *Sezione INFN di Padova, Padova, Italy*
- ²³ *Sezione INFN di Pisa, Pisa, Italy*
- ²⁴ *Sezione INFN di Roma Tor Vergata, Roma, Italy*
- ²⁵ *Sezione INFN di Roma La Sapienza, Roma, Italy*
- ²⁶ *Henryk Niewodniczanski Institute of Nuclear Physics Polish Academy of Sciences, Kraków, Poland*
- ²⁷ *AGH - University of Science and Technology, Faculty of Physics and Applied Computer Science, Kraków, Poland*
- ²⁸ *National Center for Nuclear Research (NCBJ), Warsaw, Poland*
- ²⁹ *Horia Hulubei National Institute of Physics and Nuclear Engineering, Bucharest-Magurele, Romania*
- ³⁰ *Petersburg Nuclear Physics Institute (PNPI), Gatchina, Russia*
- ³¹ *Institute of Theoretical and Experimental Physics (ITEP), Moscow, Russia*
- ³² *Institute of Nuclear Physics, Moscow State University (SINP MSU), Moscow, Russia*
- ³³ *Institute for Nuclear Research of the Russian Academy of Sciences (INR RAN), Moscow, Russia*
- ³⁴ *Budker Institute of Nuclear Physics (SB RAS) and Novosibirsk State University, Novosibirsk, Russia*
- ³⁵ *Institute for High Energy Physics (IHEP), Protvino, Russia*
- ³⁶ *Universitat de Barcelona, Barcelona, Spain*
- ³⁷ *Universidad de Santiago de Compostela, Santiago de Compostela, Spain*
- ³⁸ *European Organization for Nuclear Research (CERN), Geneva, Switzerland*
- ³⁹ *Ecole Polytechnique Fédérale de Lausanne (EPFL), Lausanne, Switzerland*
- ⁴⁰ *Physik-Institut, Universität Zürich, Zürich, Switzerland*
- ⁴¹ *Nikhef National Institute for Subatomic Physics, Amsterdam, The Netherlands*
- ⁴² *Nikhef National Institute for Subatomic Physics and VU University Amsterdam, Amsterdam, The Netherlands*
- ⁴³ *NSC Kharkiv Institute of Physics and Technology (NSC KIPT), Kharkiv, Ukraine*
- ⁴⁴ *Institute for Nuclear Research of the National Academy of Sciences (KINR), Kyiv, Ukraine*
- ⁴⁵ *University of Birmingham, Birmingham, United Kingdom*
- ⁴⁶ *H.H. Wills Physics Laboratory, University of Bristol, Bristol, United Kingdom*
- ⁴⁷ *Cavendish Laboratory, University of Cambridge, Cambridge, United Kingdom*
- ⁴⁸ *Department of Physics, University of Warwick, Coventry, United Kingdom*
- ⁴⁹ *STFC Rutherford Appleton Laboratory, Didcot, United Kingdom*
- ⁵⁰ *School of Physics and Astronomy, University of Edinburgh, Edinburgh, United Kingdom*
- ⁵¹ *School of Physics and Astronomy, University of Glasgow, Glasgow, United Kingdom*
- ⁵² *Oliver Lodge Laboratory, University of Liverpool, Liverpool, United Kingdom*
- ⁵³ *Imperial College London, London, United Kingdom*
- ⁵⁴ *School of Physics and Astronomy, University of Manchester, Manchester, United Kingdom*
- ⁵⁵ *Department of Physics, University of Oxford, Oxford, United Kingdom*
- ⁵⁶ *Massachusetts Institute of Technology, Cambridge, MA, United States*
- ⁵⁷ *University of Cincinnati, Cincinnati, OH, United States*
- ⁵⁸ *University of Maryland, College Park, MD, United States*
- ⁵⁹ *Syracuse University, Syracuse, NY, United States*
- ⁶⁰ *Pontifícia Universidade Católica do Rio de Janeiro (PUC-Rio), Rio de Janeiro, Brazil, associated to ²*
- ⁶¹ *Institute of Particle Physics, Central China Normal University, Wuhan, Hubei, China, associated to ³*
- ⁶² *Departamento de Física, Universidad Nacional de Colombia, Bogota, Colombia, associated to ⁸*
- ⁶³ *Institut für Physik, Universität Rostock, Rostock, Germany, associated to ¹¹*
- ⁶⁴ *National Research Centre Kurchatov Institute, Moscow, Russia, associated to ³¹*
- ⁶⁵ *Yandex School of Data Analysis, Moscow, Russia, associated to ³¹*
- ⁶⁶ *Instituto de Física Corpuscular (IFIC), Universitat de Valencia-CSIC, Valencia, Spain, associated to ³⁶*
- ⁶⁷ *Van Swinderen Institute, University of Groningen, Groningen, The Netherlands, associated to ⁴¹*

- ^a *Universidade Federal do Triângulo Mineiro (UFTM), Uberaba-MG, Brazil*
- ^b *P.N. Lebedev Physical Institute, Russian Academy of Science (LPI RAS), Moscow, Russia*
- ^c *Università di Bari, Bari, Italy*
- ^d *Università di Bologna, Bologna, Italy*
- ^e *Università di Cagliari, Cagliari, Italy*
- ^f *Università di Ferrara, Ferrara, Italy*
- ^g *Università di Urbino, Urbino, Italy*
- ^h *Università di Modena e Reggio Emilia, Modena, Italy*
- ⁱ *Università di Genova, Genova, Italy*
- ^j *Università di Milano Bicocca, Milano, Italy*
- ^k *Università di Roma Tor Vergata, Roma, Italy*
- ^l *Università di Roma La Sapienza, Roma, Italy*
- ^m *Università della Basilicata, Potenza, Italy*
- ⁿ *AGH - University of Science and Technology, Faculty of Computer Science, Electronics and Telecommunications, Kraków, Poland*
- ^o *LIFAELS, La Salle, Universitat Ramon Llull, Barcelona, Spain*
- ^p *Hanoi University of Science, Hanoi, Viet Nam*
- ^q *Università di Padova, Padova, Italy*
- ^r *Università di Pisa, Pisa, Italy*
- ^s *Scuola Normale Superiore, Pisa, Italy*
- ^t *Università degli Studi di Milano, Milano, Italy*
- [†] *Deceased*